Research Article | Vol. 26, No. 10 | 14 May 2018 | OPTICS EXPRESS 13561
Optics EXPRESS

Generation of intensity-tunable structural color from helical photonic crystals for full color reflective-type display

SE-UM KIM,[1] SIN-HYUNG LEE,[1] IN-HO LEE,[1] BO-YEON LEE,[1] JUN-HEE NA,[2] AND SIN-DOO LEE[1,*]

[1]*School of Electrical and Computer Engineering, Seoul National University, 1 Gwanak-ro, Gwanak-gu, Seoul 08826, South Korea*
[2]*Department of Electric, Electronic & Communication Engineering Education, Chungnam National University, 99 Deahak-ro, Yuseong-gu, Daejeon 34134, South Korea*
**lclab2@snu.ac.kr*

Abstract: A new concept of intensity-tunable structural coloration is proposed on the basis of a helical photonic crystal (HPC). The HPCs are constructed from a mixture of chiral reactive mesogens by spin-coating, followed by the photo-polymerization. A liquid crystal (LC) layer, being homogeneously aligned, is prepared on the HPCs to serve as a tunable waveplate. The electrical modulation of the phase retardation through the LC layer directly leads to the intensity-tunable Bragg reflection from the HPCs upon the incidence of the polarized light. The bandwidths of the structural colors are found to be well preserved regardless of the applied voltage. A prototype of a full color reflective-type display, incorporated with three primary color units, is demonstrated. Our concept of decoupling two mutually independent functions, the intensity modulation by the tunable waveplate and the color reflection by the HPCs provides a simple and powerful way of producing a full color reflective-type display which possesses high color purity, high optical efficiency, the cycling durability, and the design flexibility.

© 2018 Optical Society of America under the terms of the OSA Open Access Publishing Agreement

OCIS codes: (120.2040) Displays; (160.3710) Liquid crystals; (160.5298) Photonic crystals.

References and links

1. I. Ota, J. Ohnishi, and M. Yoshiyama, "Electrophoretic image display (EPID) panel," Proc. IEEE **61**(7), 832–836 (1973).
2. R. Hattori, S. Yamada, Y. Masuda, and N. Nihei, "A novel bistable reflective display using quick-response liquid powder," J. Soc. Inf. Disp. **12**(1), 75–80 (2004).
3. K.-M. H. Lenssen, P. J. Baesjou, F. P. M. Budzelaar, M. H. W. M. van Delden, S. J. Roosendaal, L. W. G. Stofmeel, A. R. M. Verschueren, J. J. van Glabbeek, J. T. M. Osenga, and R. M. Schuurbiers, "Novel concept for full-color electronic paper," J. Soc. Inf. Disp. **17**(4), 383–388 (2009).
4. S. Mukherjee, W. L. Hsieh, N. Smith, M. Goulding, and J. Heikenfeld, "Electrokinetic pixels with biprimary inks for color displays and color-temperature-tunable smart windows," Appl. Opt. **54**(17), 5603–5609 (2015).
5. R. A. Hayes and B. J. Feenstra, "Video-speed electronic paper based on electrowetting," Nature **425**(6956), 383–385 (2003).
6. J. Heikenfeld, K. Zhou, E. Kreit, B. Raj, S. Yang, B. Sun, A. Milarcik, L. Clapp, and R. Schwartz, "Electrofluidic displays using Young–Laplace transposition of brilliant pigment dispersions," Nat. Photonics **3**(5), 292–296 (2009).
7. H. You and A. J. Steckl, "Three-color electrowetting display device for electronic paper," Appl. Phys. Lett. **97**(2), 023514 (2010).
8. Z. Yi, L. Shui, L. Wang, M. Jin, R. A. Hayes, and G. Zhou, "A novel driver for active matrix electrowetting displays," Displays **37**, 86–93 (2015).
9. T.-H. Yoon, G.-D. Lee, and J. C. Kim, "Nontwist quarter-wave liquid-crystal cell for a high-contrast reflective display," Opt. Lett. **25**(20), 1547–1549 (2000).
10. C. D. Sheraw, L. Zhou, J. R. Huang, D. J. Gundlach, T. N. Jackson, M. G. Kane, I. G. Hill, M. S. Hammond, J. Campi, B. K. Greening, J. Francl, and J. West, "Organic thin-film transistor-driven polymer-dispersed liquid crystal displays on flexible polymeric substrates," Appl. Phys. Lett. **80**(6), 1088–1090 (2002).
11. Z. Ge, X. Zhu, R. Lu, T. X. Wu, and S.-T. Wu, "Transflective liquid crystal display using commonly biased reflectors," Appl. Phys. Lett. **90**(22), 221111 (2007).
12. Y. Li, D. Luo, and Z. H. Peng, "Full-color reflective display based on narrow bandwidth templated cholesteric liquid crystal film," Opt. Mater. Express **7**(1), 16–24 (2017).

#327346 https://doi.org/10.1364/OE.26.013561
Journal © 2018 Received 2 Apr 2018; revised 7 May 2018; accepted 8 May 2018; published 10 May 2018

Optics EXPRESS

13. M. W. Miles, "Interferometric modulation: MOEMS as an enabling technology for high-performance reflective displays," Proc. SPIE **4985**, 131–139 (2003).
14. J. Hong, E. Chan, T. Chang, R. Fung, C. Kim, J. Ma, Y. Pan, B. Wen, I. Reines, and C. Lee, "Single mirror interferometric display – a new paradigm for reflective display technologies," SID Symp. Dig. Tech. Papers **45**(1), 793–796 (2014).
15. K. A. Arpin, A. Mihi, H. T. Johnson, A. J. Baca, J. A. Rogers, J. A. Lewis, and P. V. Braun, "Multidimensional architectures for functional optical devices," Adv. Mater. **22**(10), 1084–1101 (2010).
16. J. N. Segal, S. Keren-Zur, N. Hendler, and T. Ellenbogen, "Controlling light with metamaterial-based nonlinear photonic crystals," Nat. Photonics **9**(3), 180–184 (2015).
17. S. Chen, K. Roh, J. Lee, W. K. Chong, Y. Lu, N. Mathews, T. C. Sum, and A. Nurmikko, "A photonic crystal laser from solution based organo-lead Iodide perovskite thin films," ACS Nano **10**(4), 3959–3967 (2016).
18. J. J. Walish, Y. Kang, R. A. Mickiewicz, and E. L. Thomas, "Bioinspired electrochemically tunable block copolymer full color pixels," Adv. Mater. **21**(30), 3078–3081 (2009).
19. T. J. Park, S. K. Hwang, S. Park, S. H. Cho, T. H. Park, B. Jeong, H. S. Kang, Y. Ryu, J. Huh, E. L. Thomas, and C. Park, "Electrically tunable soft-solid block copolymer structural color," ACS Nano **9**(12), 12158–12167 (2015).
20. L. Nucara, F. Greco, and V. Mattoli, "Electrically responsive photonic crystals: a review," J. Mater. Chem. C Mater. Opt. Electron. Devices **3**(33), 8449–8467 (2015).
21. X. Dai, Y. Xiang, S. Wen, and H. He, "Thermally tunable and omnidirectional terahertz photonic bandgap in the one-dimensional photonic crystals containing semiconductor InSb," J. Appl. Phys. **109**(5), 053104 (2011).
22. C. Markos, "Thermo-tunable hybrid photonic crystal fiber based on solution-processed chalcogenide glass nanolayers," Sci. Rep. **6**(1), 31711 (2016).
23. G. Chu, X. Wang, T. Chen, J. Gao, F. Gai, Y. Wang, and Y. Xu, "Optically tunable chiral plasmonic guest–host cellulose films weaved with long-range ordered silver nanowires," ACS Appl. Mater. Interfaces **7**(22), 11863–11870 (2015).
24. D. Gur, B. A. Palmer, B. Leshem, D. Oron, P. Fratzl, S. Weiner, and L. Addadi, "The mechanism of color change in the neon tetra fish: a light-induced tunable photonic crystal array," Angew. Chem. Int. Ed. Engl. **54**(42), 12426–12430 (2015).
25. A. C. Arsenault, T. J. Clark, G. von Freymann, L. Cademartiri, R. Sapienza, J. Bertolotti, E. Vekris, S. Wong, V. Kitaev, I. Manners, R. Z. Wang, S. John, D. Wiersma, and G. A. Ozin, "From colour fingerprinting to the control of photoluminescence in elastic photonic crystals," Nat. Mater. **5**(3), 179–184 (2006).
26. T. Ding, G. Cao, C. G. Schäfer, Q. Zhao, M. Gallei, S. K. Smoukov, and J. J. Baumberg, "Revealing invisible photonic inscriptions: images from strain," ACS Appl. Mater. Interfaces **7**(24), 13497–13502 (2015).
27. I. R. Howell, C. Li, N. S. Colella, K. Ito, and J. J. Watkins, "Strain-tunable one dimensional photonic crystals based on zirconium dioxide/slide-ring elastomer nanocomposites for mechanochromic sensing," ACS Appl. Mater. Interfaces **7**(6), 3641–3646 (2015).
28. C. Pouya, J. T. B. Overvelde, M. Kolle, J. Aizenberg, K. Bertoldi, J. C. Weaver, and P. Vukusic, "Characterization of a mechanically tunable gyroid photonic crystal inspired by the butterfly parides sesostris," Adv. Opt. Mater. **4**(1), 99–105 (2016).
29. H. Kikuchi, M. Yokota, Y. Hisakado, H. Yang, and T. Kajiyama, "Polymer-stabilized liquid crystal blue phases," Nat. Mater. **1**(1), 64–68 (2002).
30. F. Castles, F. V. Day, S. M. Morris, D.-H. Ko, D. J. Gardiner, M. M. Qasim, S. Nosheen, P. J. W. Hands, S. S. Choi, R. H. Friend, and H. J. Coles, "Blue-phase templated fabrication of three-dimensional nanostructures for photonic applications," Nat. Mater. **11**(7), 599–603 (2012).
31. T.-H. Lin, Y. Li, C.-T. Wang, H.-C. Jau, C.-W. Chen, C.-C. Li, H. K. Bisoyi, T. J. Bunning, and Q. Li, "Red, green and blue reflections enabled in an optically tunable self-organized 3D cubic nanostructured thin film," Adv. Mater. **25**(36), 5050–5054 (2013).
32. M. Stimulak and M. Ravnik, "Tunable photonic crystals with partial bandgaps from blue phase colloidal crystals and dielectric-doped blue phases," Soft Matter **10**(33), 6339–6346 (2014).
33. E. Bukusoglu, X. Wang, J. A. Martinez-Gonzalez, J. J. de Pablo, and N. L. Abbott, "Stimuli-responsive cubosomes formed from blue phase liquid crystals," Adv. Mater. **27**(43), 6892–6898 (2015).
34. J.-D. Lin, T.-Y. Wang, T.-S. Mo, S.-Y. Huang, and C.-R. Lee, "Wide-band spatially tunable photonic bandgap in visible spectral range and laser based on a polymer stabilized blue phase," Sci. Rep. **6**(1), 30407 (2016).
35. S. S. Choi, S. M. Morris, W. T. S. Huck, and H. J. Coles, "Simultaneous red-green-blue reflection and wavelength tuning from an achiral liquid crystal and a polymer template," Adv. Mater. **22**(1), 53–56 (2010).
36. Y. Inoue, H. Yoshida, H. Kubo, and M. Ozaki, "Deformation-free, microsecond electro-optic tuning of liquid crystals," Adv. Opt. Mater. **1**(3), 256–263 (2013).
37. J. P. Vernon, U. A. Hrozhyk, S. V. Serak, V. P. Tondiglia, T. J. White, N. V. Tabiryan, and T. J. Bunning, "Optically reconfigurable reflective/scattering states enabled with photosensitive cholesteric liquid crystal cells," Adv. Opt. Mater. **1**(1), 84–91 (2013).
38. K. M. Lee, V. P. Tondiglia, M. E. McConney, L. V. Natarajan, T. J. Bunning, and T. J. White, "Color-tunable mirrors based on electrically regulated bandwidth broadening in polymer-stabilized cholesteric liquid crystals," ACS Photonics **1**(10), 1033–1041 (2014).
39. M. Faryad and A. Lakhtakia, "The circular Bragg phenomenon," Adv. Opt. Photonics **6**(2), 225–292 (2014).
40. N. Y. Ha, Y. Ohtsuka, S. M. Jeong, S. Nishimura, G. Suzaki, Y. Takanishi, K. Ishikawa, and H. Takezoe, "Fabrication of a simultaneous red-green-blue reflector using single-pitched cholesteric liquid crystals," Nat. Mater. **7**(1), 43–47 (2008).

Optics EXPRESS

41. M. E. McConney, V. P. Tondiglia, L. V. Natarajan, K. M. Lee, T. J. White, and T. J. Bunning, "Electrically induced color changes in polymer-stabilized cholesteric liquid crystals," Adv. Opt. Mater. **1**(6), 417–421 (2013).
42. S.-U. Kim, B.-Y. Lee, J.-H. Suh, J. Kim, J.-H. Na, and S.-D. Lee, "Reduction of gamma distortions in liquid crystal display by anisotropic voltage-dividing layer of reactive mesogens," Liq. Cryst. **44**(2), 364–371 (2017).
43. K. Hwang, D. Kwak, C. Kang, D. Kim, Y. Ahn, and Y. Kang, "Electrically tunable hysteretic photonic gels for nonvolatile display pixels," Angew. Chem. Int. Ed. Engl. **50**(28), 6311–6314 (2011).
44. M. G. Han, C.-J. Heo, H. Shim, C. G. Shin, S.-J. Lim, J. W. Kim, Y. W. Jin, and S. Lee, "Structural color manipulation using tunable photonic crystals with enhanced switching reliability," Adv. Opt. Mater. **2**(6), 535–541 (2014).
45. Q. Zhao, A. Haines, D. Snoswell, C. Keplinger, R. Kaltseis, S. Bauer, I. Graz, R. Denk, P. Spahn, G. Hellmann, and J. J. Baumberg, "Electric-field-tuned color in photonic crystal elastomers," Appl. Phys. Lett. **100**(10), 101902 (2012).
46. J. Xiang, Y. Li, Q. Li, D. A. Paterson, J. M. D. Storey, C. T. Imrie, and O. D. Lavrentovich, "Electrically tunable selective reflection of light from ultraviolet to visible and infrared by heliconical cholesterics," Adv. Mater. **27**(19), 3014–3018 (2015).
47. J.-H. Na, H. Li, S. C. Park, and S.-D. Lee, "Symmetric-viewing liquid crystal display with alternating alignment layers in an inverse-twisted-nematic configuration," J. Inf. Disp. **12**(4), 191–194 (2011).
48. S. C. Park, J.-H. Na, and S.-D. Lee, "Colloidal particle-based surface nanotopography with high mechanical stability by thermal fixation for liquid crystal devices," J. Appl. Phys. **112**(2), 023104 (2012).
49. E.-S. Yu, S.-U. Kim, J.-H. Suh, J. Kim, J.-H. Na, and S.-D. Lee, "The domain mixing effect on the electro optical properties of liquid crystals using polyimide doped with reactive mesogen," J. Inf. Disp. **17**(3), 125–130 (2016).
50. J. Li, S.-T. Wu, S. Brugioni, R. Meucci, and S. Faetti, "Infrared refractive indices of liquid crystals," J. Appl. Phys. **97**(7), 073501 (2005).
51. J. Li, G. Baird, Y.-H. Lin, H. Ren, and S.-T. Wu, "Refractive-index matching between liquid crystals and photopolymers," J. Soc. Inf. Disp. **13**(12), 1017–1026 (2005).
52. I.-H. Lee, S.-H. Lee, C.-M. Keum, S.-U. Kim, and S.-D. Lee, "Combinatorial color arrays based on optical micro-resonators in monolithic architecture," Opt. Express **22**(12), 15320–15327 (2014).
53. C.-K. Liu, T.-H. Yang, and K.-T. Cheng, "Expanding color gamut of reflective liquid crystal displays from filtering undesirable wavelengths of a light source by an embedded etalon," Appl. Opt. **56**(7), 1880–1885 (2017).
54. L. A. Francis and K. Iniewski, *Novel Advances in Microsystems Technologies and Their Applications* (CRC Press, 2016).

1. Introduction

The increasing demand of the comfortable and superb viewing capability under diverse illuminating environments has driven the development of reflective-type displays. Such reflective-type displays can be realized by adjusting the reflectance of each pixel, thereby producing an image under ambient light. The implementation of colors in reflective-type displays typically requires a transmissive color filter array or a scheme that is capable of selectively reflecting colors. Much effort based on electrophoresis [1–4], electro-wetting [5–8], liquid crystals (LCs) [9–12], and interferometry [13,14] has been made toward the fabrication of full color reflective-type displays but it is still challenging to overcome the color loss, the insufficient color depth, and the low reflectivity.

Recently, photonic crystals (PCs) have drawn a great deal of interest as a new candidate for the color elements [15–17]. The structural colors from the PCs can be tuned by manipulating either the lattice constant or the refractive index by means of electrical [18–20], thermal [21,22], optical [23,24], and mechanical stimuli [25–28]. Those approaches necessarily involve the deformations of the structure formed in a solid, implying that the wide tuning range, the fast response, and the cycling durability are substantially limited in such case. Even in the case of LC-type PCs such as the blue phases [29–34] or the chiral phases [35–38] that allow band-widening and band-shifting, the PCs are very diffusive in nature and easily distorted under electrical perturbations as well as external heat and pressure. Moreover, the intensity-tuning capability of the structural colors, which is indispensable for full color reflective-type displays, has rarely been achieved so far. Thus, it is essential to search for a new type of the coloration mechanism for use in high-performance color reflective-type displays and other sophisticated color systems.

Optics EXPRESS

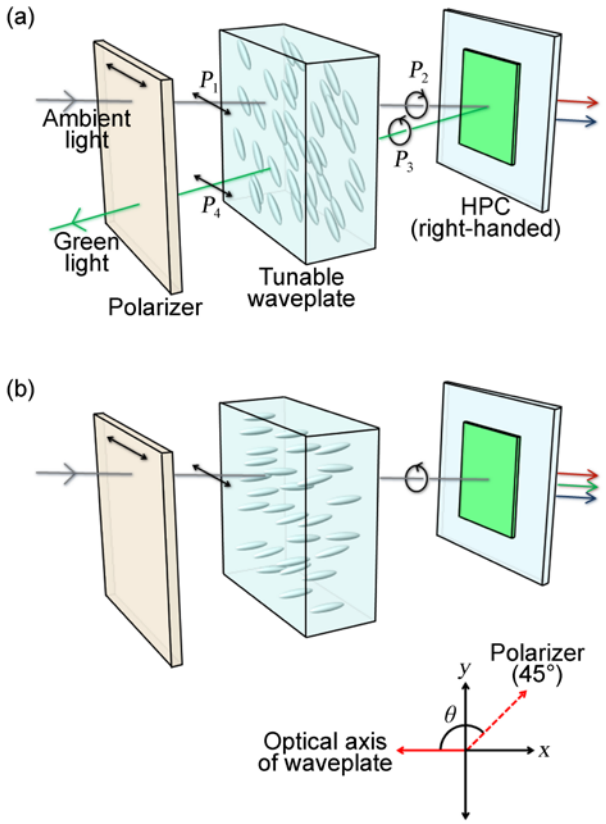

Fig. 1. Operation principle of the intensity-tunable structural coloration based on the HPC. Color unit consists of the front polarizer, the homogeneously aligned LC layer (a tunable waveplate), and the HPC: (a) The voltage-off state (total reflection state) that the incident light becomes circularly polarized in the same direction as the handedness of the HPC and a certain bandwidth of the incident light corresponding to the Bragg reflection of the HPC comes out from the incidence plane. Here, P_1, P_2, P_3, and P_4 denote the polarization states of the light in the optical stages. (b) The voltage-on state (total transmission state) that the incident light becomes circularly polarized in the opposite direction to the handedness of the HPC by the reorientation of the LC molecule and penetrates the HPC without the Bragg reflection. Here, θ denotes the angle between the optical axis of the tunable waveplate and the front polarizer.

In this work, we propose a novel concept of the intensity-tunable structural colors which can be directly applicable for full color reflective-type displays. The basic idea relies on the reflectivity modulation from a helical photonic crystal (HPC) according to the polarization of the incident light. The coloration unit consists of the HPC, a tunable waveplate, and the front polarizer. The HPC was constructed using a mixture of chiral reactive mesogens (CRMs) by spin-coating and the subsequent photo-polymerization under the exposure of the ultraviolet (UV) light. The HPC leads to Bragg reflection of the incident light which is circularly polarized in the same handedness of the helix. An array of the HPCs for the three primary red (R), green (G), and blue (B) structural colors (HPC-R, HPC-G, and HPC-G, respectively) was simply produced from three different mixtures of the CRMs having different concentrations of the chiral dopant. Note that a relatively high concentration of the chiral dopant in the mixture of the CRMs results in the blue shift of the bandwidth. On the top of the HPCs, a homogeneously aligned LC layer was prepared to serve as a tunable waveplate through which the phase retardation of the polarized incident light varies with the applied voltage. The variations of the phase retardation directly yield those of the reflectance from the HPCs. According to the value of the phase retardation (Φ) through the LC layer and the angle (θ) between the optical axis of the tunable waveplate and the front polarizer, the incident light

Optics EXPRESS

becomes circularly polarized in the same direction as the handedness of the HPC and a certain bandwidth of the incident light, corresponding to the Bragg reflection of the HPC, comes out from the incidence plane in the voltage-off state or the incident light is oppositely polarized by the reorientation of the LC molecules and penetrates the HPC without the Bragg reflection when the applied voltage is high as shown in Figs. 1(a) and 1(b), respectively.

2. Experimental

2.1 Material preparation

Solutions of acrylate-based CRMs (RMS11-066, RMS11-067, and RMS11-068; Merck) in toluene were used in this study. The central Bragg wavelengths of the uniform films of RMS11-066, RMS11-067, and RMS11-068, prepared by spin-coating, drying, and UV curing, were about 424 nm, 530 nm, and 631 nm, respectively.

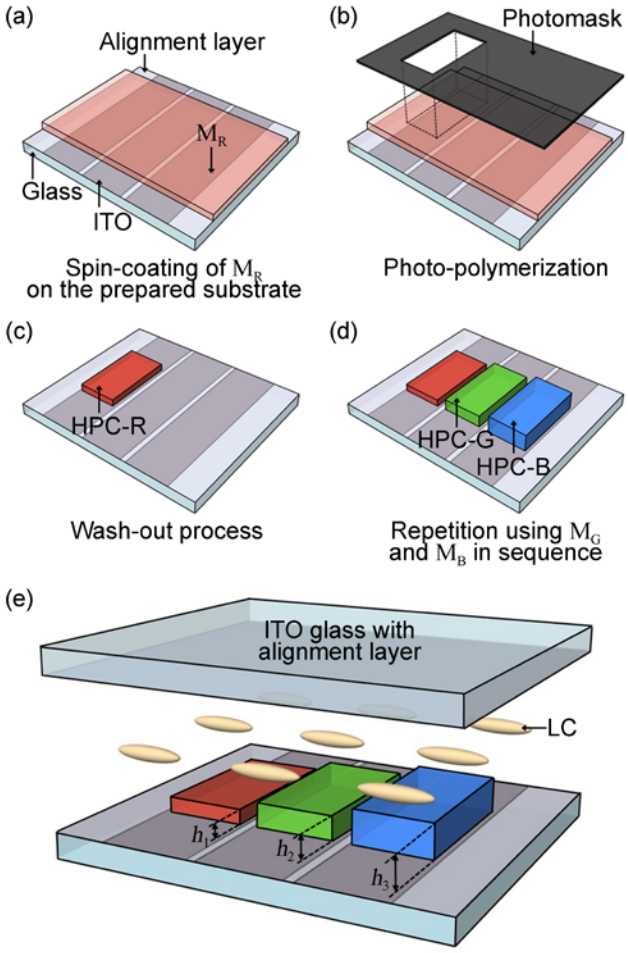

Fig. 2. Fabrication of the color reflective-type display based on the HPC array: (a) Spin-coating of M_R on the bottom substrate. Top and bottom substrates were prepared by patterning ITO electrode and applying a homogeneous alignment layer. (b) Photo-polymerization of M_R with the photomask. (c) Wash-out process for un-polymerized material. (d) Repetition of spin-coating, photo-polymerization, and wash-out process using M_G and M_B for the construction of HPC-G and HPC-B, respectively. (e) Assembly of the top substrate and injection of LC as the tunable waveplate. Here, h_1, h_2, and h_3 denote the thickness of the HPC-R, HPC-G, and HPC-B, respectively.

Optics EXPRESS

Three mixtures for R, G, and B colorations (M_R, M_G, and M_B, respectively) were prepared by blending two solutions among RMS11-066, RMS11-067, and RMS11-068. M_R was made up of RMS11-067 and RMS11-068 in a weight ratio of 1:9. M_G is a mixture of RMS11-067 and RMS11-068 in a weight ratio of 9:1. M_B is a mixture of RMS11-066 and RMS11-067 in a weight ratio of 7:3. The central Bragg wavelengths of the polymerized films of M_R, M_G, and M_B were 620 nm, 540 nm, and 460 nm, respectively.

2.2 Fabrication process

As shown in Fig. 2, an array of R, G, and B color units was constructed inside the LC cell to form a monolithic configuration, called the in-cell type, for our color reflective-type display. A homogeneous alignment layer (AL22620, JSR) for the LC material was spin-coated on the inner surface of indium-tin-oxide patterned glass substrates at the rate of 3000 rpm for 30 s and post-annealed at 180°C for 1 h. The rubbing directions on the top and bottom substrates were anti-parallel to each other. For the construction of the HPC-R, M_R was spin-coated at the rate of 3500 rpm for 30 s on the bottom substrate and dried at 55°C for 60 s to remove the residual solvent. The layer of M_R was then photo-polymerized through a photo-mask under the exposure of ultraviolet light at the intensity of 20 mW/cm^2 for 120 s. The un-polymerized M_R was washed out in toluene (Sigma Aldrich Korea) and fully dried at 75°C. HPC-G and HPC-B were similarly constructed using M_G and M_B, respectively. The thickness of the HPCs was varied by adjusting the spin-coating rate. The LC cell gap was maintained to be 3.5 μm using glass spacers. The LC with the positive dielectric anisotropy, E7 (n_e = 1.7305, Δn = + 0.2116; Merck), was infiltrated the cell by the capillary action. A front polarizer was placed on the top glass substrate so that θ had several different values (θ = 15°, 45°, 90°, 135°, and 165°).

3. Geometrical analysis

We first performed the numerical simulations of the transmittance and the reflectance for one of three primary colors (G color) as a function of Φ and θ. The amplitude and the polarization state of the light were calculated by the 2 × 2 Jones matrix method. The essential features are basically the same for other two colors (R and B). We used a right-handed (RH) HPC which can be considered as a left-handed circular (LHC) polarizer for the transmitted light and a RH circular (RHC) polarizer for the reflected light. The incident light is the unpolarized light with the intensity of I_{in}. The angle of the front polarizer is set to be 45° with respect to the x axis. The angle of its optical axis with respect to the x axis is denoted by θ_o. Thus, the angle (θ) between the optical axis of the tunable waveplate and the front polarizer simply becomes θ_o–45°. First the polarization of the incident light after the tunable waveplate (P_2) is expressed as

$$P_2 = \frac{I_{in}}{\sqrt{2}}\begin{bmatrix} \cos^2\theta_o - \cos\theta_o \sin\theta_o + e^{i\Phi}\left(\sin^2\theta_o + \cos\theta_o \sin\theta_o\right) \\ \sin^2\theta_o - \cos\theta_o \sin\theta_o + e^{i\Phi}\left(\cos^2\theta_o + \cos\theta_o \sin\theta_o\right) \end{bmatrix}. \tag{1}$$

The polarization state for the transmitted light (P_t) is then described as

$$P_t = \frac{K_t I_{in}}{2\sqrt{2}}\begin{bmatrix} 1 \\ -i \end{bmatrix}, \tag{2}$$

where

$$\begin{aligned} K_t = {} & \cos^2\theta_o - \cos\theta_o \sin\theta_o + i\left(-\sin^2\theta_o + \cos\theta_o \sin\theta_o\right) \\ & + e^{i\Phi}\left(\sin^2\theta_o + \cos\theta_o \sin\theta_o\right) - ie^{i\Phi}\left(\cos^2\theta_o + \cos\theta_o \sin\theta_o\right). \end{aligned} \tag{3}$$

The transmitted intensity (I_t) for the input intensity (I_{in}) in terms of Φ and θ is given by

Optics EXPRESS

$$\frac{I_t}{I_{in}} = \frac{1-\sin 2\theta \sin \Phi}{4}. \tag{4}$$

The polarization state for the reflected light from the HPC (P_3) can be described as

$$P_3 = \frac{K_r I_{in}}{2\sqrt{2}}\begin{bmatrix} 1 \\ -i \end{bmatrix}, \tag{5}$$

where

$$\begin{aligned} K_r = {} & \cos^2\theta_o - \cos\theta_o \sin\theta_o + i\left(\sin^2\theta_o - \cos\theta_o \sin\theta_o\right) \\ & + e^{i\Phi}\left(\sin^2\theta_o + \cos\theta_o \sin\theta_o\right) + ie^{i\Phi}\left(\cos^2\theta_o + \cos\theta_o \sin\theta_o\right). \end{aligned} \tag{6}$$

During the reverse propagation mode, the angles of optical axis and the front polarizer have opposite sign. The polarization state for the reflected light after the tunable waveplate (P_4) can be described as

$$P_4 = \frac{K_r I_{in}}{2\sqrt{2}}\begin{bmatrix} \cos^2\theta_o - \cos\theta_o \sin\theta_o + e^{i\Phi}\left(\sin^2\theta_o + \cos\theta_o \sin\theta_o\right) \\ \sin^2\theta_o - \cos\theta_o \sin\theta_o + e^{i\Phi}\left(\cos^2\theta_o + \cos\theta_o \sin\theta_o\right) \end{bmatrix}. \tag{7}$$

The polarization state for the reflected light observed at the incident plane (P_r) corresponds to the linear polarization component at –45° of P_4,

$$P_r = \frac{K_r^2 I_{in}}{4\sqrt{2}}\begin{bmatrix} 1 \\ -1 \end{bmatrix}. \tag{8}$$

Finally, the reflected intensity (I_r) for the input intensity (I_{in}) in terms of Φ and θ is given by

$$\frac{I_r}{I_{in}} = \frac{1}{2}\left[\frac{1+\sin 2\theta \sin \Phi}{2}\right]^2. \tag{9}$$

The contour plots of Eq. (4) and Eq. (9) in 2-dimensional space of θ and Φ were shown in Figs. 3(a) and 3(c), respectively. For θ = 135°, the reflectance varies from 0.5 to 0 as Φ varies from $3\pi/2$ to $\pi/2$. Since the phase retardation decreases with increasing the applied voltage, the normally white state is obtained at θ = 135°. In contrast, for θ = 45°, the normally black state is achieved. Figures 3(b) and 3(d) show the experimental results of the transmittance and the reflectance, respectively. Note that the peak wavelength of the HPC was chosen to match with the wavelength (λ = 534 nm) of a monochromic light source used in the experiment. The amount of the phase modulation was derived from the voltage-dependent reflectance. The measurements were carried out for several different values of θ (θ = 15°, 45°, 90°, 135°, and 165°). The experimental results were found to be in good agreement with the numerical simulations. The observed deviations are attributed to the tilt variations of the incident angle of the light and/or the mismached phase modulation due to the cell gap error. It is well known that the shift of the peak wavelength of the HPC is in accordance with the angle of the incident light [39]. The reflected light then propagates along the longer optical pathway so that the phase retardation increases. This limits the range of the color gamut to some extent. The polarization state along the optical pathway can be systematically described on the Poincaré sphere as shown in Fig. 3(e). The angle of the front polarizer is 45° with respect to the x axis. The value of θ is 135° and Φ is in the range from $3\pi/2$ to $\pi/2$. First, P_1 is the linear polarization at 45° with respect to the x axis and it corresponds to + S_2. During the light propagation through the tunable waveplate (P_1 to P_2), the polarization state rotates clockwise (CW) by the amount of Φ. Since the RH HPC reflects only the RHC polarization component of P_2, P_3 becomes the RHC polarization (+ S_3). The reflected light follows the same optical

Optics EXPRESS

pathway as that for the incident light. P_4 appears after the CW rotation by the amount of Φ from + S_3. The angle between the front polarizer and the reflected light is –45° (-S_2).

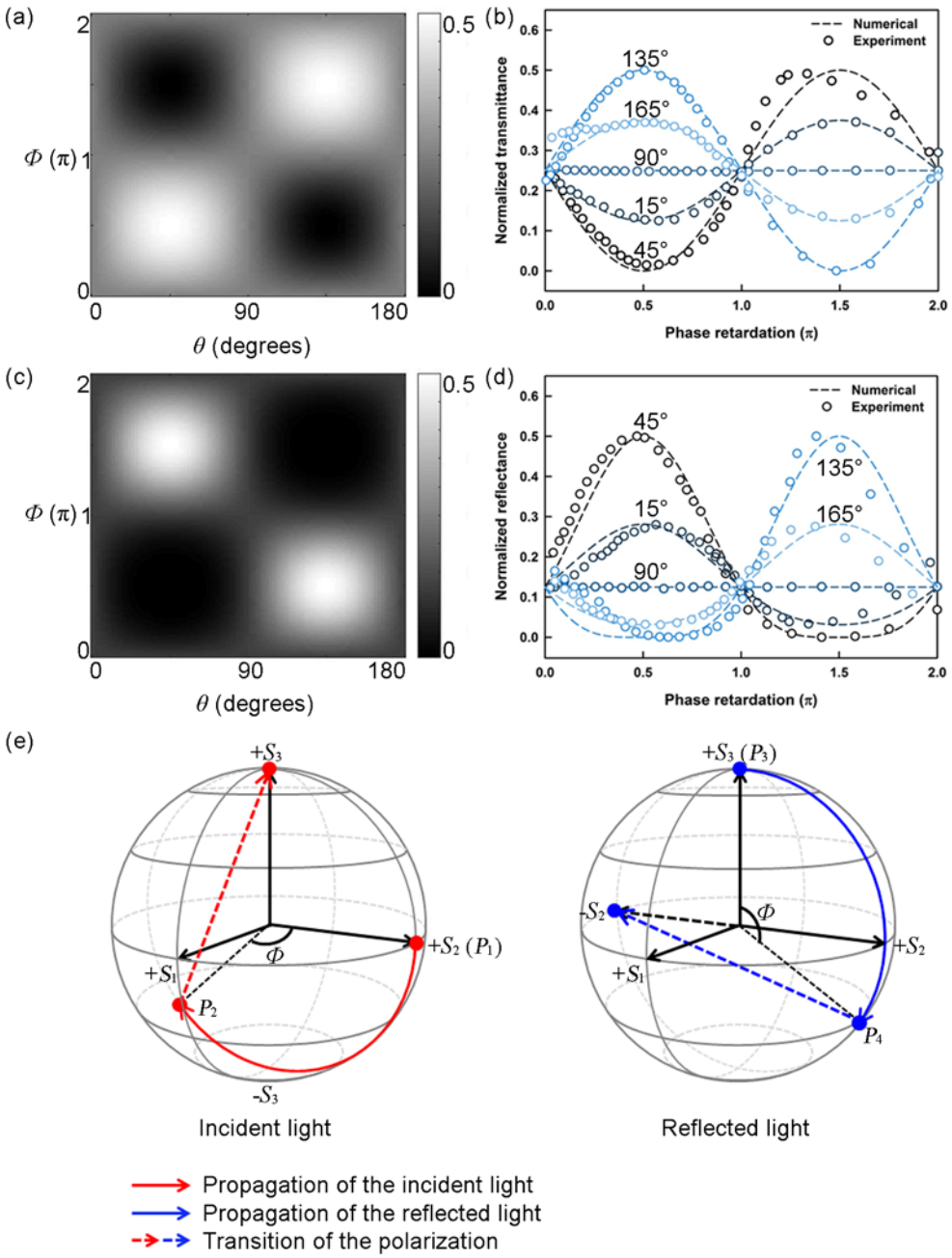

Fig. 3. Numerical and the experimental results of the transmittance and the reflectance of the G unit as a function of θ and Φ: (a) The contour plot of the transmittance. (b) The experimental result of the transmittance for several different values of θ (θ = 15°, 45°, 90°, 135°, and 165°). (c) The contour plot of the reflectance. (d) The experimental result of the reflectance for several different values of θ (θ = 15°, 45°, 90°, 135°, and 165°). (e) Poincaré spheres showing the polarization states along the optical pathway for θ = 135°. The red and blue arrows represent the propagation of the incident light and that of the reflected light, respectively. The dashed arrows represent the transitions of the polarization states.

Optics EXPRESS

Finally, the linear polarization component at −45° of P_4 comes out from the device. In the initial state ($\Phi = 3\pi/2$), P_2, P_3, and P_4 simply become + S_3, + S_3, and -S_2, respectively, with no loss of the intensity. For $\Phi = \pi/2$, P_2 is orthogonal to + S_3 so that no reflection occurs at all. This optical configuration is applicable for other types of devices constructed using different materials or different types of patterns. In our device, the thickness of the HPC (h_k, k = 1, 2, 3, representing R, G, and B color) in three primary color unit yielding 3π/2 phase retardation for each color is given by

$$h_k = d - \frac{3\lambda_k}{4\Delta n}, \tag{10}$$

where d is the thickness of the cell gap and λ_k is the central Bragg wavelength of the HPC (λ_1 = 620 nm, λ_2 = 540 nm, and λ_3 = 460 nm). In our case that d was chosen to be 3.5 μm, the thickness of HPC-R (h_1), HPC-G (h_2), and HPC-B (h_3) were about 1.3 μm, 1.6 μm, and 1.9 μm, respectively. Note that the thickness of each HPC should be at least twice larger than the helical pitch of the HPC so as to produce the corresponding structural colors [40,41].

4. Electro-optical properties

Figure 4(a) shows the reflectance as a function of the applied voltage.

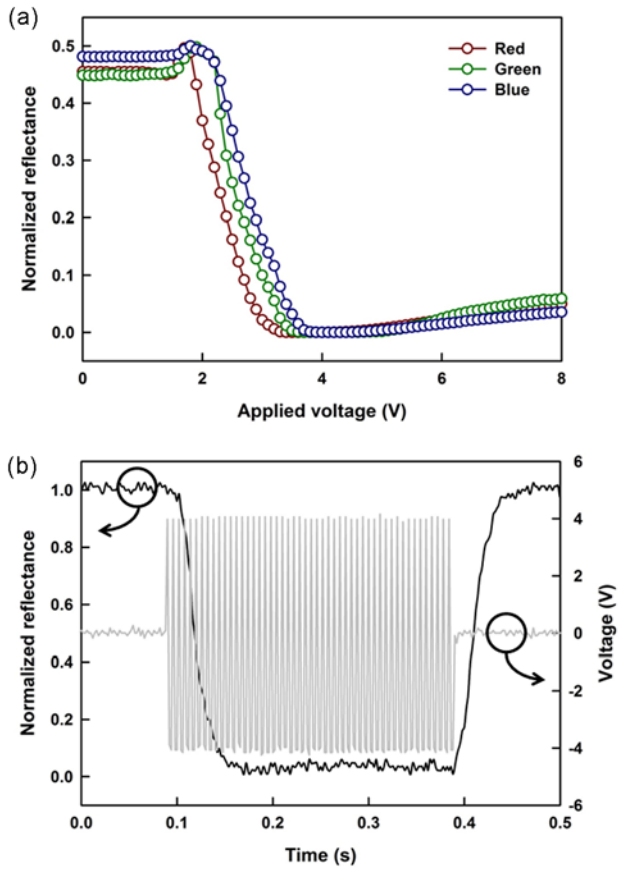

Fig. 4. Electro-optical properties of three color units (R, G, and B): (a) The voltage-dependent reflectance of R, G, and B color units. (b) Dynamic response of the R color unit. The applied voltage was a bipolar square waveform with the amplitude of 4 V at the frequency of 1 kHz.

The coherent light source was used for measuring the reflectance of R, G, and B color units at the peak wavelengths of 633 nm, 543 nm, and 465 nm, respectively. It should be

Optics EXPRESS

noted that the voltage division by the HPC decreases the effective voltage applied to the LC layer [42]. Therefore, the operating voltage increases as the thickness of the HPC increases. The slight increase in the reflectance around the threshold voltage was originated from the thickness mismatch of the LC layer.

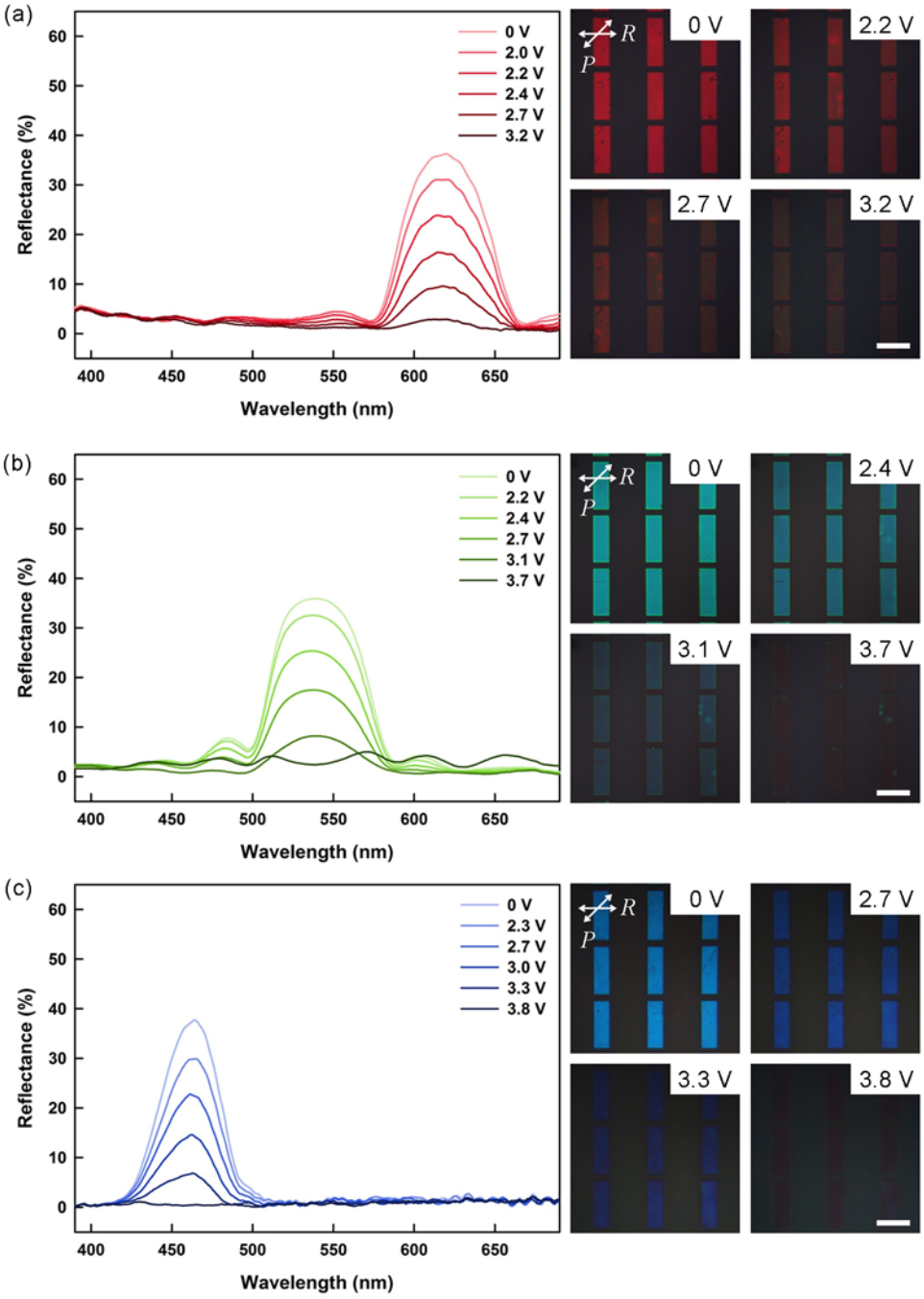

Fig. 5. Reflection spectra showing the intensity-tuning capability of (a) R, (b) G, and (c) B color units and the corresponding POM images of the arrays of the color units at several different values of the applied voltage. Here, *P* and *R* denote the optic axis of the front polarizer and the rubbing direction, respectively. Scale bars in the POM images are 200 μm.

Optics EXPRESS

The gradual increase in the reflectance above 4 V was observed since the phase retardation became smaller than π/2. Figure 4(b) shows the dynamic response of the R color unit, measured using a He-Ne laser with the wavelength of 633 nm in conjunction with a digitizing oscilloscope (Waverunner 6040, Lecroy). The applied voltage was a bipolar square waveform with the amplitude of 4 V at the frequency of 1 kHz from a function generator (DS 345, Stanford Research Systems). The rising and falling times were estimated from the normalized reflectance curve (from 10% to 90% and vice versa) and they were 46 ms and 64 ms, respectively. Those are much faster than the previous cases based on the electrical stimuli [20,43–46], but slower than the typical response of the LC molecules [47,48]. The relatively weak anchorage at the HPC is likely to slow down the dynamic response of the LC compared to the strong anchorage in the top alignment layer [49]. The optical dispersion of E7 used in our study, depending on the wavelength, is quite small. Like typical LC materials, however, the temperature-dependence of the refractive index will cause the decrease of the effective refractive index [50,51].

Figure 5 shows the tunable reflection spectra and the corresponding microscopic images of three color units (R, G, and B) at several applied voltages, obtained with a polarizing optical microscope (POM). The width and the length of each color unit were 100 μm and 300 μm, respectively. The separation between two adjacent color units was about 200 μm. Although the LC alignment might be somewhat disturbed at the surface of the HPC, the LC molecules were found to be uniformly aligned along the rubbing direction in the top alignment layer. This may result from the fact that the anchoring strength is relatively weak at the surface of the HPC than the top alignment layer. A deuterium halogen light source and a UV-Visible fiber optic spectrometer (Ocean Optics S2000) were used for measuring the reflection spectra. The homogeneous LC cell with no HPC was used as the reference. The bandwidth of R, G, and B color units were measured to be 460 ± 42 nm, 540 ± 43 nm, and 620 ± 42 nm as shown in Figs. 5(a), 5(b), and 5(c), respectively. The measured reflectivity (about 38%) was lower than the theoretical value (50%) due to the refraction at the interfaces. As the applied voltage increases, the intensity decreases but the peak wavelength and the bandwidth were well preserved irrespective of the applied voltage. Our concept of decoupling two mutually independent functions, the intensity modulation by the tunable waveplate and the color reflection by the HPCs, led to the achievement of high optical efficiency and high uniformity of coloration. This manifests itself the unique features of our HPC-based coloration compared to existing approaches where the deformation of PCs have been widely used for the band-widening and band-shifting. Regarding the off-axis viewing, the difference in the effective optical pathway through the tunable waveplate at different incident angles will result in the variance of the color depth. The arbitrary incident angle may experience the blue shift of the reflection spectrum so that color deviation may be observed. It should be noted that conventional color filters suffer intrinsically from the deterioration of the reflectivity and the color gamut since the incident light and the reflected light pass different color filters placed on the top of devices [52,53].

Another important point is that for the the generation of the color depth, in contrast to multiple area-weighted pixels [54], our single color unit-based approach is capable of modulating the color intensity. As a result, this intensity-tuning capability allows a relatively small pixel dimension, depending only on the resolution of the photomask for fabication, and the scalability of resolution. The light leakage observed in some of the color units resulted from the deterioration of the chiral nature of the CRM directors.

Finally, we constructed a prototype of a full color reflective-type display based on the three primary color units as shown in Fig. 6. The HPC-R, the HPC-G, and the HPC-B were patterned to show three letters of “S”, “N”, and “U” and arranged in three groups of R, G, and B colors on the bottom substrate. The applied voltages of V_R, V_G, and V_B correspond to R, G, and B color groups, respectively. As shown in Fig. 6(a), the bright states for all three structural colors were achieved under no applied voltage (V_R = 0 V, V_G = 0 V, and V_B = 0 V). When V_R, V_G, or V_B was applied independently to the device, the dark state for R, G, or B color was accordingly obtained. For example, when V_R = 0 V, V_G = 0 V, and V_B = 3.8 V, the

Optics EXPRESS

incident light was totally transmitted through the HPC-B and thus the characters of B color were not visible from the front of the device as shown in Fig. 6(b). Similarly, the characters of G color were not visible as shown in Fig. 6(c) when V_R = 0 V, V_G = 3.7 V, and V_B = 0 V. As shown in Fig. 6(d), the characters of R color were not seen when V_R = 3.2 V, V_G = 0 V, and V_B = 0 V. Except for the HPC patterns for coloration, other regions with only the homogeneous LC layer remain always in the dark state regardless of the applied voltage. Those regions act spontaneously as the black matrices that are used for the separation between the adjacent pixels. Our prototype device meets the practical requirements for a full color reflective display such as the low voltage operation, the relatively fast response, the high optical efficiency, and the intensity-tunable structural colors.

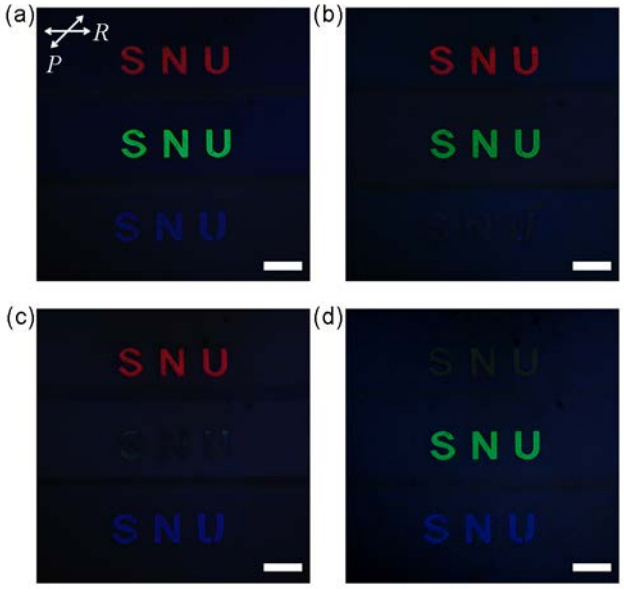

Fig. 6. The demonstration of a prototype of a full color reflective-type display incorporated with three primary color units. The POM images showing (a) the bright state for three color units in the initial state (V_R = 0 V, V_G = 0 V, and V_B = 0 V), and the black states for (b) B color unit (V_R = 0 V, V_G = 0 V, and V_B = 3.8 V), (c) G color unit (V_R = 0 V, V_G = 3.7 V, and V_B = 0 V), and (d) R color unit (V_R = 3.2 V, V_G = 0 V, and V_B = 0 V). Scale bars are 200 μm.

5. Concluding remarks

We proposed a novel concept of the intensity-tunable structural coloration based on the HPCs in a monolithic configuration. Basic color units were produced from the mixtures of the CRMs through spin-coating and the intensity-tuning capability was achieved from a tunable waveplate of the LC layer. The reflectance from the color unit, depending on the phase retardation through the LC layer, was in good agreement with the polarization analysis on the Poincaré sphere. Note that our proposed configuration theoretically achieves the highest reflectance (50%) in a very simple scheme which needs only one linear polarizer and a tunable waveplate. The band widths of the reflection spectra were well preserved during the intensity-tuning of the structural colors. A prototype of a full color reflective-type display indeed demonstrated the intensity-tuning capability of vivid structural colors. Our approach will offer a practical and feasible way of building up a new class of visual systems such as digital signage, camouflage, and smart windows.

Acknowledgments

This work was supported in part by the Nanjing Sea Star Blue Display Technology Center.

69.245.71.222 (ts 2018-08-02 03:15:06)